RSC Sustainability

Accepted Manuscript

This article can be cited before page numbers have been issued, to do this please use: Y. Huang, C. Do-Thanh, Z. Yang, S. Dai and H. Chen, *RSC Sustainability*, 2026, DOI: 10.1039/D5SU00861A.

ROYAL SOCIETY OF CHEMISTRY

View Article Online
DOI: 10.1039/D5SU00861A

The excessive use of single-use plastics, due to their persistence and slow degradation, has generated significant environmental, economic, and health concerns. In this work, we developed a tandem cross-linking/carbonization route for converting polyethylene (PE) into advanced carbon materials. Subsequent carbonization yields high-quality nanoporous carbons with surface areas up to 2080 $m^2 g^{-1}$, outperforming previous plastic-to-carbon methods. The resulting materials exhibit excellent performance in gas separation and energy storage applications.

View Article Online
DOI: 10.1039/D5SU00861A

COMMUNICATION

Tectonic approach for waste-to-nanomaterial transformation towards polyethylene recycling

Received 00th January 20xx,
Accepted 00th January 20xx

DOI: 10.1039/x0xx00000x

Yanan Huang,[a] Chi-Linh Do-Thanh,[b] Zhenzhen Yang,*[c] Sheng Dai,*[b,c] Hao Chen,*[a,b]

Polyethylene (PE) wastes were recycled into nanoporous carbon materials via $NaNH_2$-catalyzed tandem cross-linking and carbonization. The process enables C–H cleavage and C–N formation, yielding carbons with surface areas up to 2080 m^2 g^{-1}. The resulting materials exhibit excellent performance in gas separation and energy storage applications.

The overconsumption of single-use plastics with long lifetimes, slow decomposition rates, and ecosystem disruption potentials has brought widespread environmental, economic, and health concerns.[1-3] Compared to mechanical recycling, landfilling, and incineration, selective conversion of the single-use plastics in the presence of heterogeneous, homogeneous, or biocatalytic systems represents promising research efforts towards wastes recycling into value-added chemicals (building blocks), advanced materials (carbons), and fuels (liquid hydrocarbons), deploying polyethylene (PE), polypropylene (PP), polyethylene terephthalate (PET), polyurethane (PU), polyvinyl chloride (PVC), or polystyrene (PS), as starting materials.[3, 4] For example, via pyrolysis, PE recycling in the presence of $CuCO_3$,[5] or PP recycling in the presence of zeolites (e.g., HY-2.8 or NaY-2.8) could generate liquid hydrocarbons.[6, 7] Heterogeneous metal nanocatalysts capable of activating H_2 have been demonstrated in hydrocracking of PE (e.g., $Pt/SiTiO_3$ or SiO_2/Pt)[8, 9] or mixed plastic waste (e.g., Al-SBA-15)[10] to generate motor oil or liquid hydrocarbons. Dehydrochlorination of PVC[11] or glycolysis of PET[12, 13] could produce the corresponding monomers. Besides these aspects obtaining small molecular chemicals or liquid products, gasification–carbonization of PP, PE, or PET could also form carbonaceous nanomaterials. In the presence of organically modified montmorillonite-based catalytic systems (no additive or doped by Co_3O_4, NiO), plastic recycling could be achieved to generate graphene flakes, hollow carbon spheres, or multi-wall carbon nanotubes (MWCNTs).[14-17] Carbonization of mixed plastic waste catalyzed by Ni/Al_2O_3 led to the formation of CNTs.[18] Heterostructures composed of carbon and metal oxides (e.g., Fe_3O_4@C core shell structures) were obtained from PE in the presence of ferrocene and ammonium carbonate.[19, 20] Although progress has been made, the utilization of plastic wastes to produce high-quality carbon materials is still highly underexplored. Especially, high catalyst loading (up to 800 wt%), requirement of metal additives, and inferior porosity of the carbonaceous products restricted the application of the plastic-to-carbon strategies in energy-related fields. Particularly, compared with PET, PU, and PVC containing extra ester, urea, or halide moieties, high- and low-density polyethylene (HDPE and LDPE), and PP solely composed of strong single C–C and C–H bonds within the plastic skeleton exhibited higher thermodynamic stability and kinetic inertness, leading to energy-intensive and low efficient recycling outcomes even under rigorous conditions.[1] Facile approaches capable of producing high-quality nanoporous carbons deploying PE-based starting materials will represent a critical forefront in the discovery of cost-effective and high-performance plastic-to-material pathways towards energy-related applications.

Herein, a tandem cross-linking and carbonization pathway was developed towards the transformation of PE to advanced materials (**Figure 1**). Sodium amide ($NaNH_2$) with its strong basicity and nucleophilic activity was deployed as the catalyst for C–H bond cleavage in the PE skeleton and new C–N bond construction, leading to cross-linking of the PE precursor and enhanced thermal stability, which was then carbonized via thermal treatment into high-quality nanoporous carbon materials with surface areas up to 2080 m^2 g^{-1}, surpassing those obtained via the previously demonstrated procedures for plastic waste carbonization. The high surface area and abundant micropores within the carbon skeletons gave the as-

[a] State Key Laboratory for Chemo and Biosensing, College of Chemistry and Chemical Engineering, Hunan University, Changsha, 410082, China.
[b] Department of Chemistry, Institute for Advanced Materials and Manufacturing, University of Tennessee, Knoxville, TN 37996, USA.
[c] Chemical Sciences Division, Oak Ridge National Laboratory, Oak Ridge, TN 37831, USA.
* Corresponding author.
E-mail address: chenhaoch@hnu.edu.cn (H. Chen), yangz3@ornl.gov (Z. Yang), dais@ornl.gov (S. Dai)

View Article Online
DOI: 10.1039/D5SU00861A

afforded materials impressive performance in CO_2 capture/separation and energy storage as the component in supercapacitor construction. This study provides new insight into the PE recycling to afford promising material candidates in energy-related fields.

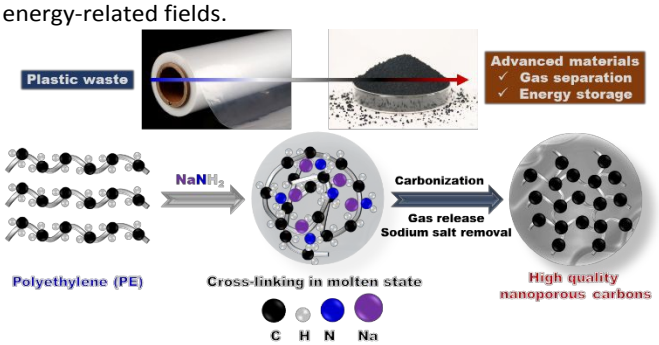

Figure 1. Schematic illustration of the PE recycling by $NaNH_2$-promoted cross-linking/carbonization to produce advanced materials.

Screening of the reaction parameters was then conducted using the surface area of the carbon products as an indicator, which is an important feature in the fields of gas uptake, catalysis, and energy storage. Taking PE with molecular weight of 3000 as the precursor, which was pyrolyzed from 410 to 480 °C (**Figure S1A**) with the sphere-like morphology as shown in **Figure S1B**, and $NaNH_2$ as the catalyst, different carbon materials are fabricated by varying the catalyst loading and reaction temperature. The as-prepared carbon materials are denoted as C-m-T (m = mass ratio of $NaNH_2$:PE, T = reaction temperature). The Brunauer–Emmett–Teller (BET) surface area of the products is analysed by N_2 absorption at 77 K (**Figure 2A and Figure S1C, Figure S2 and S3**). The N_2 adsorption–desorption isotherms of the PE precursor, showing a nearly featureless profile with extremely low adsorption capacity, indicating its non-porous or very weakly porous nature. With the reaction temperature of 850 °C, C-0.1-850 obtained with $NaNH_2$:PE mass ratio of 0.1 showed a surface area of 703 $m^2\ g^{-1}$ while increasing the loading amount of $NaNH_2$ led to an enhanced surface area, with C-0.25-850 exhibiting a surface area of 1450 $m^2\ g^{-1}$ being collected. However, further increasing the $NaNH_2$:PE mass ratio had an inferior effect on the surface area of the carbon products, leading to the formation of C-0.5-850 and C-0.75-850 with surface areas of 1033 and 630 $m^2\ g^{-1}$, respectively. These results indicated that a $NaNH_2$:PE mass ratio of 0.25 is optimal to generate carbon materials with high surface areas. Creation of the porosity with the carbon skeleton was possibly due to the gas formation and release (e.g., H_2, CH_4, and NH_3) upon C–C bond construction during the reaction procedure in the presence of $NaNH_2$.[21] The diminished surface area of carbons in the presence of high loading amount of $NaNH_2$ was probably owing to collapse of the nanoporous structures driven by the strong basicity of the amide anion and partial decomposition of the carbon moieties. Combined with the Raman spectra (Figure S4), two characteristic bands centered at ~1350 and ~1580 cm^{-1}, corresponding to the D and G bands of carbonaceous species, are clearly observed for C-0.1-850. The prominent D and G signals indicate the presence of defect-rich sp^2 carbon domains formed during the thermal treatment.[22] With the mass ratio of $NaNH_2$:PE increased, the intensities of both bands decrease significantly, suggesting the formation of more disordered carbon structures. TGA results indicate that an appropriate amount of $NaNH_2$ enhances the thermal stability of the carbon materials, whereas excessive $NaNH_2$ loading leads to a decrease in thermal stability (Figure S5). Subsequently, the influence of reaction temperature was studied using a $NaNH_2$:PE mass ratio of 0.25 in the range of 550–950 °C. The successful carbonization of PE was achieved at reaction temperature of 550 °C with a carbon yield of 25%, generating C-0.25-550 with a surface area of 451 $m^2\ g^{-1}$. Increasing the reaction temperature to 650 and 750 °C only showed slight improvement on the porosity of the carbon products, with C-0.25-650 (carbon yield: 28%) and C-0.25-750 (carbon yield: 30%) having surface areas of 562 and 733 $m^2\ g^{-1}$, respectively, being obtained. Comparatively, C-0.25-850 synthesized at 850 °C exhibited significantly increased surface area (1450 $m^2\ g^{-1}$). However, further increasing the reaction temperature to 950 °C resulted in a slight decrease of the surface area in C-0.25-950 (1228 $m^2\ g^{-1}$) and carbon yield (20%). Detailed characterization of C-0.25-850 with the highest surface area was conducted to determine more structure information. The powder X-ray diffraction (PXRD) pattern of the PE precursor exhibited a crystalline structure, which, upon cross-linking and decomposition in the presence of $NaNH_2$ and at high temperature, became an amorphous carbon product (C-0.25-850) (**Figure S6**). Comparison of the Fourier-transform infrared spectroscopy (FTIR) indicated the complete loss of the aliphatic C–H moieties within the skeleton of C-0.25-850, which was clearly shown around 2900 cm^{-1} in the PE precursor (**Figure S7**), demonstrating the high catalytic efficiency of $NaNH_2$ in cleavage of the C–H bonds during thermal treatment procedure. X-ray photoelectron spectroscopy (XPS) analysis showed that C-0.25-850 was composed of carbon and nitrogen, with the latter only occupying 0.8 at.% on the surface. Therefore, most of the nitrogen moieties was released in the form of gaseous products via decomposition at high temperature. The C1s spectrum of C-0.25-850 could be deconvoluted into three major peaks with binding energy (BE) of 284.71, 286.21, and 288.48 eV, corresponding to the carbon atoms in C–C, C–N, and C=NH^+, respectively (**Figure 2B**).[23] This is in accordance with the N1s spectrum, with two major peaks at BE = 398.45 (C–N) and 399.98 eV (C=NH^+). The N_2 adsorption and desorption isotherms of C-0.25-850 showed a type I reversible profile (**Figure 2C**), which exhibited steep N_2 sorption at low pressure region (< 0.01 bar) derived from the existence of micropores. Pore size distribution curves calculated by the nonlocal density functional theory (NLDFT) method demonstrated the presence of micropores around 0.53 and 1.0–2.0 nm **(Figure 2D**). The total surface area (1450 $m^2\ g^{-1}$) was dominated by micropore area (1051 $m^2\ g^{-1}$), and a small amount of external surface area (399 $m^2\ g^{-1}$). Correspondingly, the total pore volume of 0.93 $cm^3\ g^{-1}$ composing 0.42 $cm^3\ g^{-1}$ from micropores. Scanning electron microscopy (SEM) showed that C-0.25-850 was composed of particles with sphere-like morphology and smooth surface structure (**Figure 2E**). Transmission electron microscopy (TEM) images further confirm the sphere-like particles with some of

View Article Online
DOI: 10.1039/D5SU00861A

them containing hollow space and existence of porous structures (**Figure 2F**). With the achievement made using PE with molecular weight of 3000 as the precursor, the $NaNH_2$-promoted carbonization procedure was further extended to PE with high molecular weight (35000). With a $NaNH_2$:PE_{35000} mass ratio of 0.25 and reaction temperature of 850 °C, the as-afforded carbon material was denoted as C'-0.25-850, which had amorphous morphology indicated by the PXRD pattern (**Figure S8**) and showed no characteristic signals for C–H bonds in the FTIR spectrum (**Figure S9**). Porosity analysis by N_2 sorption isotherms revealed that C'-0.25-850 had an improved surface area (2080 m^2 g^{-1}) compared with the carbon product from PE_{3000} under the same conditions (**Figure 2G**), with 551 m^2 g^{-1} derived from the micropore area and 1529 m^2 g^{-1} from the external surface area. The total pore volume was 1.14 cm^3 g^{-1}, with 0.25 cm^3 g^{-1} contributed by micropore. The pore size distribution curve calculated from the NLDFT method exhibited the co-existence of micropores (< 2 nm) and mesopores (2–4 nm) (**Figure 2H**). All the above-mentioned results demonstrated the high catalytic activity of $NaNH_2$ in activation and cleavage of the C–H bond in PE and formation of the C–C bond in construction of carbon skeleton. Specifically, $NaNH_2$ acts as a strong nucleophilic species that can initiate C–H bond activation in PE via deprotonation-driven cleavage.[24] This process generates highly reactive carbon-centered intermediates, which subsequently undergo dehydrogenation and radical-like cross-linking reactions, thereby accelerating the formation of a more interconnected carbon framework.[25] With only a catalytic amount of catalyst and without other templates or additives, high-quality nanoporous carbon materials could be afforded with surface areas surpassing the PE-generated carbon materials by other methodologies (**Table S1**), most of the polymer-derived carbons using hard/soft templates[26] and even carbon materials activated by excess amounts of $NaNH_2$ (e.g., 2 equivalents).[25]

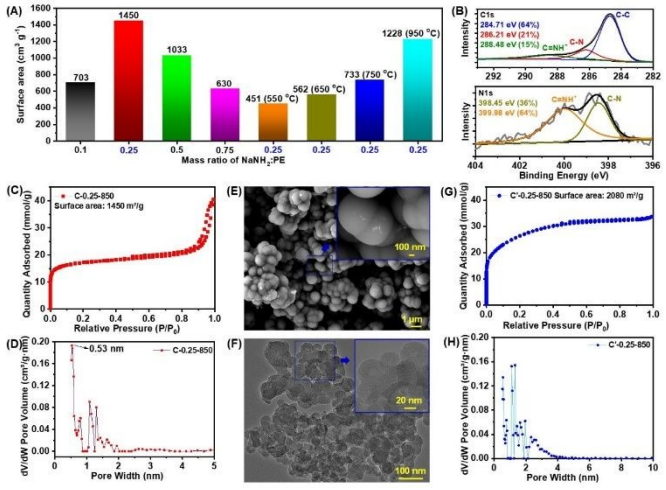

Figure 2 (A) Surface area of the carbon materials obtained with different mass ratio of $NaNH_2$:PE and reaction temperature. (B) C1s and N1s XPS spectra, (C) N_2 sorption and desorption isotherms (77 K), (D) pore size distribution curve, (E) SEM images, and (F) TEM images of C-0.25-850. (G) N_2 sorption and desorption isotherms and (H) pore size distribution curve of C'-0.25-850.

Carbonaceous materials have shown wide applications in the field of gas storage, separation, catalysis, and energy storage.[26, 27] CO_2 capture and sequestration (CCS) represents one of the most intensively studied technologies towards alleviating the global greenhouse gas impact.[28-32] Nanomaterials with high surface areas and involvement of micro- or ultra-micropores are preferred capable of achieving high CO_2 uptake capacity and selectivity.[33, 34] The as-prepared carbon materials in PE recycling exhibited high surface areas up to 2080 m^2 g^{-1} and abundant micropores within the skeleton, which made them promising candidates in CO_2 capture and separation. The CO_2 uptake isotherms of the nanoporous carbon materials are collected at 273 and 29 K (**Table S2, Figure 3A and 3B**), among which C-0.25-850 exhibited the highest CO_2 uptake capacity. As shown in **Figure 3A**, the CO_2 uptake capacity of C-0.25-850 achieved 5.31 and 3.32 mmol g^{-1} at 273 and 298 K, respectively, which was higher than most of the carbon-based materials as reported in the literatures,[35-39] and comparable to the capacity of nitrogen-doped systems (**Table S2**).[40-42] The CO_2/N_2 selectivity was calculated to be 27 and 24 at 273 and 298 K, respectively, by the ideal adsorption solution theory (IAST) with the ratio of N_2: CO_2 as 85: 15. The isosteric heat of adsorption (Q_{st}) was calculated to be 27.8 kJ mol^{-1} for C-0.25-850 (**Figure 3C**). Comparatively, the CO_2 uptake capacity of C'-0.25-850 with higher surface area (2080 m^2 g^{-1}) didn't surpass that obtained by C-0.25-850 (5.21 mmol g^{-1} at 273 K, 1 bar; 3.53 mmol g^{-1} at 298 K, 1 bar) because the C-0.25-850 contained a larger fraction of micropores (especially pores <0.7 nm), which exhibit stronger affinity toward CO_2 molecules (kinetic diameter ≈ 0.33 nm)[43, 44] and therefore deliver higher uptake at low pressures. In contrast, although C'-0.25-850 possesses a higher BET surface area than C-0.25-850, its adsorption in the low-pressure region is much less pronounced (Figure G), suggesting that the additional surface area mainly originates from mesopores/macropores or pore structures that are unfavorable for strong CO_2 adsorption.The CO_2/N_2 selectivity of C'-0.25-850 was calculated to be 41 and 30, respectively, together with Q_{st} of 19.5 kJ mol^{-1}. The CO_2 capture results demonstrated that via the $NaNH_2$-promoted cross-linking and carbonization procedure, the stable plastic wastes are transformed into advanced materials as good adsorbents in CO_2 capture and separation.

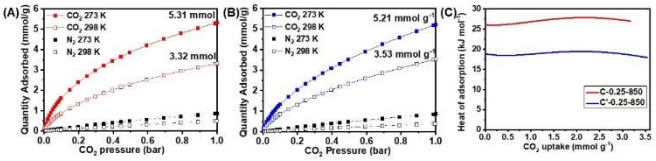

Figure 3 (A) CO_2 and N_2 isotherms of C-0.25-850 at 273 and 298 K. (B) CO_2 and N_2 isotherms of C'-0.25-850 at 273 and 298 K. (C) Heat of adsorption of C-0.25-850 and C'-0.25-850 in CO_2 capture.

The high surface areas and abundant porosity involvement of the as-afforded carbon materials prompted us to further explore their applications in energy storage. Among diverse devices, supercapacitors featured by high power density, good reversibility, wide operating temperature, and long cycle life

View Article Online
DOI: 10.1039/D5SU00861A

have attracted extensive attention being deployed as critical components in frequency modulator, tube voltage-stabilizing, consumer electronics, and hybrid electric vehicles.[45-48] Supercapacitors are categorized as electrical double-layer capacitors (EDLCs) and pseudocapacitors, in which the charge storage mechanism occurs via physical electrostatic adsorption and reversible surface chemical redox reactions, respectively.[49] EDLCs generally display enhanced power density, improved stability in extreme heat or cold conditions, and prolonged cycling life than pseudocapacitors. Material skeletons composed of sp^2 carbons, featured by high surface area, appropriate pore size distribution, good conductivity, and excellent chemical stability are preferred for promising electrode materials in EDLCs.[50, 51] The unique features of the

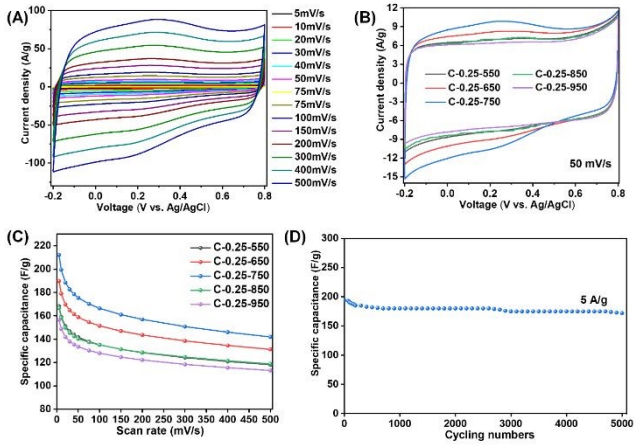

Figure 4 (A) CV curves of C-0.25-750 at different scan rates from 5 to 500 mV s^{-1}. (B) CV curves of C-0.25-T (T = heating temperature) at 50 mV s^{-1}. (C) CV rate performances of C-0.25-T. (D) GCD long cycle performance of C-0.25-750 at 5 A g^{-1}.

nanoporous carbon materials generated from PE recycling in this work enable them to be promising candidates in supercapacitors. The capacitive behaviors were evaluated in the three-electrode system using 1 M aqueous H_2SO_4 electrolyte with a Ag/AgCl reference electrode and a platinum counter electrode. Taking C-0.25-750 with a surface area of 733 m^2 g^{-1} as an example, all the collected cyclic voltammetry (CV) curves at different scan rates of 5–500 mV s^{-1} exhibited symmetric rectangular shapes with weakly broadened humps appearing at potentials of 0–0.6 V (**Figure 4A**), demonstrating the combination of EDLCs and pseudocapacitances.[52] Then PE-derived carbon materials (with a mass ratio of 0.25 for $NaNH_2$: PE) generated under various conditions were evaluated at 50 mV s^{-1} (**Figure 4B**). The hump increased from C-0.25-550 to C-0.25-750 and then diminished in C-0.25-850 and C-0.25-950, with the maximum value being achieved by C-0.25-750, probably owing to the decreased amounts of heteroatoms within the skeleton at higher temperatures. These heteroatoms provide additional pseudocapacitance and improve electrode wettability, which outweigh the effect of surface area alone. With higher temperatures (850–950 °C) treating, the content of heteroatom in carbon materials decreases significantly, leading to reduced pseudocapacitive contribution despite the larger BET surface area.[53, 54] The electrochemical impedance spectroscopy (EIS) measurements results show a clear decrease in charge-transfer resistance with increasing activation temperature from 550 to 750 °C, which then increased as the active temperature increased from 750 to 950 °C. This trend is fully consistent with the capacitance measurements, where samples with higher porosity and conductivity exhibit superior electrochemical performance (**Figure S10**). Correspondingly, the optimal capacitance was obtained by C-0.25-750, which was calculated to be 212.2 and 141.9 F g^{-1} at a scan rate of 5 and 500 mV s^{-1}, respectively, with a 67% retention at the higher scan rate (**Figure 4C**). Persistent cycling performance was evaluated using C-0.25-750 by the chronopotentiometric charge/discharge tests. The capacitance retention of 88.6% for more than 5000 cycles (**Figure 4D**) was maintained at a high constant current density of 5 A g^{-1}. All these results demonstrated that using the single-use plastic waste as the raw material, the facile $NaNH_2$-promoted carbonization pathway led to the generation of high-quality carbon materials acting as promising components in the field of energy storage.

In conclusion, by deploying a suitable catalyst, the PE precursor easily decomposed under inert atmosphere is capable of transforming into nanoporous carbon materials. The key lies in the cross-linking of the PE chains first to improve its thermal stability and then generation of the nanoporous materials via high-temperature thermal treatment. This facile strategy allows the successful transformation of discarded plastics to advanced materials with good performance in gas separation and energy storage.

Yanan Huang: Conceptualization, Methodology, Software, Data curation, Writing - original draft . **Chi-Linh Do-Thanh:** Software, Data curation, Writing - review & editing. **Zhenzhen Yang:** Funding acquisition, Project administration, Writing - review & editing. **Hao Chen:** Supervision, Funding acquisition, Project administration, Writing - review & editing. **Sheng Dai:** Supervision, Funding acquisition, Project administration, Writing - review & editing. All authors discussed the results and commented on the manuscript.

Conflicts of interest

There are no conflicts to declare.

Data availability

All data supporting the findings of this study are available within the article and its Supplementary Information file.

Notes and references

1 A. J. Martín; C. Mondelli; S. D. Jaydev; J. Pérez-Ramírez. *Chem* 2021, **7** (6), 1487-1533.
2 J. R. Jambeck; R. Geyer; C. Wilcox; T. R. Siegler; M. Perryman; A. Andrady; R. Narayan; K. L. Law. *Science* 2015, **347** (6223), 768.

3 M. Haussler; M. Eck; D. Rothauer; S. Mecking. *Nature* 2021, **590** (7846), 423-427.
4 X. Jiao; K. Zheng; Z. Hu; S. Zhu; Y. Sun; Y. Xie. *Adv Mater* 2021, e2005192.
5 M. V. Singh; S. Kumar; M. Sarker. *Sustain. Energy Fuels* 2018, **2** (5), 1057-1068.
6 W. Zhao; S. Hasegawa; J. Fujita; F. Yoshii; T. Sasaki; K. Makuuchi; J. Sun; S.-i. Nishimoto. *Polym Degrad Stabil* 1996, **53** (1), 129-135.
7 M. Blazsó. *J Anal Appl Pyrol* 2005, **74** (1), 344-352.
8 G. Celik; R. M. Kennedy; R. A. Hackler; M. Ferrandon; A. Tennakoon; S. Patnaik; A. M. LaPointe; S. C. Ammal; A. Heyden; F. A. Perras; et al. *ACS Cent. Sci.* 2019, **5** (11), 1795-1803.
9 A. Tennakoon; X. Wu; A. L. Paterson; S. Patnaik; Y. Pei; A. M. LaPointe; S. C. Ammal; R. A. Hackler; A. Heyden; I. I. Slowing; et al. *Nature Catalysis* 2020, **3** (11), 893-901.
10 D. Munir; Abdullah; F. Piepenbreier; M. R. Usman. *Powder Technol* 2017, **316**, 542-550.
11 A. Seino; T. Nishizaki; Y. Kanda; M. Sugioka; Y. Uemichi. *J Jpn Pet Inst* 2009, **52** (2), 70-71.
12 M. Imran; D. H. Kim; W. A. Al-Masry; A. Mahmood; A. Hassan; S. Haider; S. M. Ramay. *Polym Degrad Stabil* 2013, **98** (4), 904-915.
13 F. R. Veregue; C. T. Pereira da Silva; M. P. Moisés; J. G. Meneguin; M. R. Guilherme; P. A. Arroyo; S. L. Favaro; E. Radovanovic; E. M. Girotto; A. W. Rinaldi. *ACS Sustainable Chem Eng* 2018, **6** (9), 12017-12024.
14 T. Tang; X. Chen; X. Meng; H. Chen; Y. Ding. *Angew Chem Int Ed* 2005, **44** (10), 1517-1520.
15 J. Gong; J. Liu; X. Wen; Z. Jiang; X. Chen; E. Mijowska; T. Tang. *Ind Eng Chem Res* 2014, **53** (11), 4173-4181.
16 J. Gong; J. Liu; Z. Jiang; X. Chen; X. Wen; E. Mijowska; T. Tang. *Appl Catal B-Environ* 2014, **152-153**, 289-299.
17 Y. Yuan; Z. Xie; K. K. Turaczy; S. Hwang; J. Zhou; J. G. Chen. *Chem & Bio Engineering* 2024, **1** (1), 67-75.
18 R.-X. Yang; K.-H. Chuang; M.-Y. Wey. *Energ Fuel* 2015, **29** (12), 8178-8187.
19 J. Zhang; B. Yan; S. Wan; Q. Kong. *Ind Eng Chem Res* 2013, **52** (16), 5708-5712.
20 N. A. Elessawy; E. M. El-Sayed; S. Ali; M. F. Elkady; M. Elnouby; H. A. Hamad. *J. Water Process Eng.* 2020, **34**, 101047.
21 J. Wang; S. Kaskel. *J Mater Chem* 2012, **22** (45), 23710-23725.
22 S. I. Moseenkov; V. L. Kuznetsov; N. A. Zolotarev; B. A. Kolesov; I. P. Prosvirin; A. V. Ishchenko; A. V. Zavorin. *Materials* 2023, **16** (3).
23 Z. Yang; T. Wang; H. Chen; X. Suo; P. Halstenberg; H. Lyu; W. Jiang; S. M. Mahurin; I. Popovs; S. Dai. *ACS Energy Lett.* 2020, **6** (1), 41-51.
24 R. A. Woltornist; Y. Ma; R. F. Algera; Y. Zhou; Z. Zhang; D. B. Collum. *Synthesis (Stuttg)* 2020, **52** (10), 1478-1497.
25 K. Huang; S.-H. Chai; R. T. Mayes; S. Tan; C. W. Jones; S. Dai. *Microporous and Mesoporous Materials* 2016, **230**, 100-108.
26 H. Wang; Y. Shao; S. Mei; Y. Lu; M. Zhang; J. K. Sun; K. Matyjaszewski; M. Antonietti; J. Yuan. *Chem Rev* 2020, **120** (17), 9363-9419.
27 M. R. Benzigar; S. N. Talapaneni; S. Joseph; K. Ramadass; G. Singh; J. Scaranto; U. Ravon; K. Al-Bahily; A. Vinu. *Chem Soc Rev* 2018, **47** (8), 2680-2721.
28 S. J. Datta; C. Khumnoon; Z. H. Lee; W. K. Moon; S. Docao; T. H. Nguyen; I. C. Hwang; D. Moon; P. Oleynikov; O. Terasaki; et al. *Science* 2015, **350** (6258), 302-306.
29 R. Monastersky. *Nature* 2013, **497**, 13.
30 S. Zeng; X. Zhang; L. Bai; X. Zhang; H. Wang; J. Wang; D. Bao; M. Li; X. Liu; S. Zhang. *Chem Rev* 2017, **117** (14), 9625-9673.
31 K. Sumida; D. L. Rogow; J. A. Mason; T. M. McDonald; E. D. Bloch; Z. R. Herm; T.-H. Bae; J. R. Long. *Chem Rev* 2011, **112** (2), 724-781.
32 A. S. Palakkal; S. A. Mohamed; J. Jiang. *Chem & Bio Engineering* 2024, **1** (11), 970-978.
33 W. Gao; S. Liang; R. Wang; Q. Jiang; Y. Zhang; Q. Zheng; B. Xie; C. Y. Toe; X. Zhu; J. Wang; et al. *Chem Soc Rev* 2020, **49** (23), 8584-8686.
34 A. E. Creamer; B. Gao. *Environ Sci Technol* 2016, **50** (14), 7276-7289.
35 K. Huang; S.-H. Chai; R. T. Mayes; G. M. Veith; K. L. Browning; M. A. Sakwa-Novak; M. E. Potter; C. W. Jones; Y.-T. Wu; S. Dai. *Chem Commun* 2015, **51** (97), 17261-17264.
36 P. Puthiaraj; Y.-R. Lee; W.-S. Ahn. *Chem Eng J* 2017, **319**, 65-74.
37 N. A. Rashidi; S. Yusup. *Journal of Cleaner Production* 2017, **168**, 474-486.
38 N. S. Nasri; U. D. Hamza; S. N. Ismail; M. M. Ahmed; R. Mohsin. *Journal of Cleaner Production* 2014, **71**, 148-157.
39 L. Wang; R. T. Yang. *The Journal of Physical Chemistry C* 2012, **116** (1), 1099-1106.
40 Y. Boyjoo; Y. Cheng; H. Zhong; H. Tian; J. Pan; V. K. Pareek; J.-F. Lamonier; M. Jaroniec; J. Liu. *Carbon* 2017, **116**, 490-499.
41 L. Yue; Q. Xia; L. Wang; L. Wang; H. DaCosta; J. Yang; X. Hu. *J Colloid Interface Sci* 2018, **511**, 259-267.
42 L. Yue; L. Rao; L. Wang; L. An; C. Hou; C. Ma; H. DaCosta; X. Hu. *Energ Fuel* 2018, **32** (6), 6955-6963.
43 Y. S. Bae; R. Q. Snurr. *Angew Chem Int Ed Engl* 2011, **50** (49), 11586-11596.
44 T. Phenomena; R. Bird; W. Stewart; E. Lightfoot. *AIChE Journal* 2004, **7** (2).
45 J. R. Miller; P. Simon. *Science* 2008, **321** (5889), 651.
46 D. Kong; Y. Gao; Z. Xiao; X. Xu; X. Li; L. Zhi. *Adv Mater* 2019, **31** (45), e1804973.
47 W. Raza; F. Ali; N. Raza; Y. Luo; K.-H. Kim; J. Yang; S. Kumar; A. Mehmood; E. E. Kwon. *Nano Energy* 2018, **52**, 441-473.
48 H. Chen; Z. Yang; W. Guo; J. R. Dunlap; J. Liang; Y. Sun; K. Jie; S. Wang; J. Fu; S. Dai. *Adv Funct Mater* 2019, **29** (50), 1906284.
49 L. L. Zhang; X. Zhao. *Chem Soc Rev* 2009, **38** (9), 2520-2531.
50 L. Zhang; X. Yang; F. Zhang; G. Long; T. Zhang; K. Leng; Y. Zhang; Y. Huang; Y. Ma; M. Zhang. *J Am Chem Soc* 2013, **135** (15), 5921-5929.
51 R. Dash; J. Chmiola; G. Yushin; Y. Gogotsi; G. Laudisio; J. Singer; J. Fischer; S. Kucheyev. *Carbon* 2006, **44** (12), 2489-2497.
52 K. Wang; N. Zhao; S. Lei; R. Yan; X. Tian; J. Wang; Y. Song; D. Xu; Q. Guo; L. Liu. *Electrochim Acta* 2015, **166**, 1-11.
53 K. Huang; S. H. Chai; R. T. Mayes; G. M. Veith; K. L. Browning; M. A. Sakwa-Novak; M. E. Potter; C. W. Jones; Y. T. Wu; S. Dai. *Chem Commun (Camb)* 2015, **51** (97), 17261-17264.
54 H. M. Jeong; J. W. Lee; W. H. Shin; Y. J. Choi; H. J. Shin; J. K. Kang; J. W. Choi. *Nano Lett.* 2011, **11** (6), 2472-2477.

View Article Online
DOI: 10.1039/D5SU00861A

Data availability

The data supporting this article have been included as part of the supplementary information (SI). Supplementary information is available.